Proceedings of MNHMT2009
ASME 2009 2nd Micro/Nanoscale Heat & Mass Transfer International Conference
December 18-21, 2009, Shanghai, China

MNHMT2009-18552

CVD GROWTH, OPTICAL AND THERMAL CHARACTERIZATION OF VERTICALLY-ALIGNED SINGLE-WALLED CARBON NANOTUBES

Shigeo Maruyama and Rong Xiang

Department of Mechanical Engineering, The University of Tokyo,
7-3-1 Hongo, Bunkyo-ku, Tokyo 113-8656, Japan

ABSTRACT

Vertically aligned single-walled carbon nanotubes (VA-SWNTs) is expected to be an extra-ordinal material for various optical, electrical, energy, and thermal devices. The recent progress in growth control and characterization techniques will be discussed. The CVD growth mechanism of VA-SWNTs is discussed based on the *in-situ* growth monitoring by laser absorption during CVD. The growth curves are characterized by an exponential decay of the growth rate from the initial rate determined by ethanol pressure. The initial growth rate and decay of it are discussed with carbon over-coat on metal catalysts and gas phase thermal decomposition of precursor ethanol. For the precisely patterned growth of SWNTs, we recently propose a surface-energy-difference driven selective deposition of catalyst for localized growth of SWNTs. For a self assembled monolayer (SAM) patterned Si surface, catalyst particles deposit and SWNTs grow only on the hydrophilic regions. The proposed all-liquid-based approach possesses significant advantages in scalability and resolution over state-to-the-art techniques, which we believe can greatly advance the fabrication of nano-devices using high-quality as-grown SWNTs. The optical characterization of the VA-SWNT film using polarized absorption, polarized Raman, and photoluminescence spectroscopy will be discussed. Laser-excitation of a vertically aligned film from top means that each nanotube is excited perpendicular to its axis. Because of this predominant perpendicular excitation, interesting cross-polarized absorption and confusing and practically important Raman features are observed. The extremely high and peculiar thermal conductivity of single-walled carbon nanotubes has been explored by non-equilibrium molecular dynamics simulation approaches. The thermal properties of the vertically aligned film and composite materials are studied by several experimental techniques and Monte Carlo simulations based on molecular dynamics inputs of thermal conductivity and thermal boundary resistance. Current understanding of thermal properties of the film is discussed.

INTRODUCTION

Synthesis of vertically aligned single-walled carbon nanotubes (VA-SWNTs) was first reported (1) in early 2004 using a technique based on alcohol catalytic chemical vapor deposition (ACCVD) (2). Many other methods were developed soon after, such as water-assisted (3), oxygen-assisted (4), microwave plasma (5), and molecular beam (6) synthesis. Among these methods, the ACCVD method is arguably the simplest, and unique in that the catalyst can be applied by various methods such as the original dip-coating method (7) and combinatorial sputtering deposition (8, 9). In this paper, we use a solution-based dip-coating method (7) that has been shown to produce monodisperse nanoparticles (10) with diameters of approximately 2 nm. Some advantages of this wet approach include deposition of a very small amount of metal catalyst, as well as excellent potential for low-cost scalability. We also extend this wet process to tailor the key structural parameters of the SWNTs array, including diameter, length, and growth location of the SWNTs. Specifically, the patterned growth of SWNTs by patterning of SiO_2 layer (11) and by patterning self-assembled monolayer (SAM) film (12). The first approach (11) is the conventional concept of using SiO_2 patterned Si substrates to selectively grow 3D carbon nanotube structures. High-quality VA-SWNT patterns can be easily obtained by this protocol. Apart from the sintering of catalyst into Si at high temperature, the difference in surface wettability between Si and SiO_2 also plays an important role in this selective growth, which leads us to a novel method of patterning the growth on chemically modified surfaces. The latter approach (12) is based on the substrate wettability, which is found to be critical for the yield of SWNTs. On an OH-terminated hydrophilic Si/SiO_2 surface, the growth can be promoted by 10 times, but can be completely suppressed on a CH_3-terminated hydrophobic surface. Selective surface modification is utilized to localize the growth of SWNTs. The

proposed technique has advantages in improved simplicity and potentially better resolution compared to conventional lithography. Related to our previous finding that no-flow ACCVD is suited for growth of longer VA-SWNTs (13), some updated understanding of the decomposition of ethanol in ACCVD is also presented (14).

CVD GENERATION TECHNIQUE

The SWNT arrays used in this study were synthesized by the ACCVD method (2), where typically cobalt and molybdenum nanoparticles were loaded onto a silicon or quartz substrate by a liquid-based dip-coat method (7). The details and procedures have been described in previous reports (1, 15, 16, 17, 18) but essentially involve two dip-coating steps-once in a Mo solution, and once in a Co solution- followed by low-pressure alcohol CVD at 700-800 °C. Each dip-coat step is followed by calcinations in air for 5 min at 500 °C. Synthesis by this method has been shown to be a root-growth process (19), with catalyst nanoparticles remaining on the substrate surface and SWNTs growing perpendicular to the substrate. The growth process has been investigated using an *in situ* optical absorbance measurement (15), which shows the growth rate decays exponentially from an initial maximum. The resulting VA-SWNT arrays typically have a thickness of 10-30 μm, and consist of small bundles of ten or fewer SWNTs (20). The diameters range from 0.8 to 3.0 nm, with an average diameter of 2.0 nm (20). Our standard synthesis conditions are 800 °C and 1.4 kPa (10 Torr) of ethanol at a flow rate of 450 sccm. Standard catalyst concentrations are 0.01 wt% of both Mo and Co. The catalyst nanoparticles are reduced under 40 kPa (300 Torr) of 3% H_2 (Ar balance) during heating of the CVD chamber, but the Ar/H_2 flow is stopped prior to the introduction of ethanol.

GROWTH DYNAMICS

The growth condition and growth mechanism of VA-SWNTs is explored based on the *in-situ* growth monitoring by laser absorption during CVD (15, 17). As shown in Fig. 1, film thickness L of VA-SWNTs film at various temperature, flow-rate, and pressure can be well fit by an empirical equation:

$$L = \gamma_0 \tau \left(1 - \exp(-t/\tau)\right)$$

where γ_0 and τ are initial growth rate and growth decay time, respectively. The initial growth rate γ_0 is linearly proportional to pressure up to the critical pressure which is determined by temperature (17). This result indicates the first order reaction below the critical pressure.

Recently developed removal and transfer technique of this film (21) enabled a direct TEM observation of free-standing vertically aligned SWNTs along the alignment direction. It was revealed that the film is comprised primarily of small SWNT bundles, typically containing 3-8 SWNTs (20). This minimum

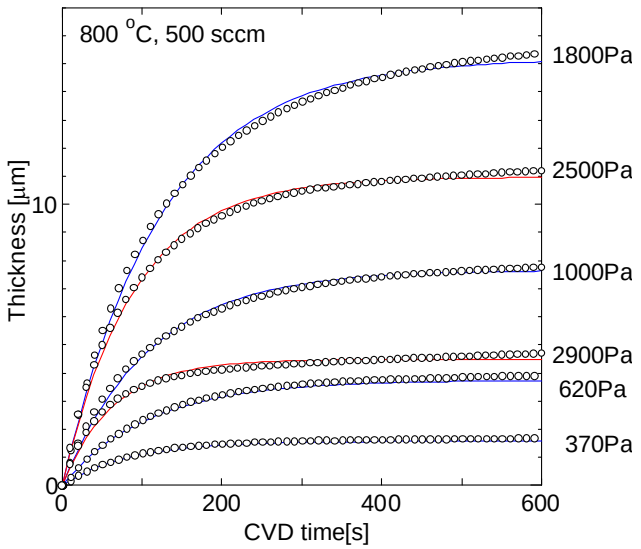

Fig. 1. *In-situ* measurement of film thickness of vertically aligned SWNTs by laser absorption during CVD.

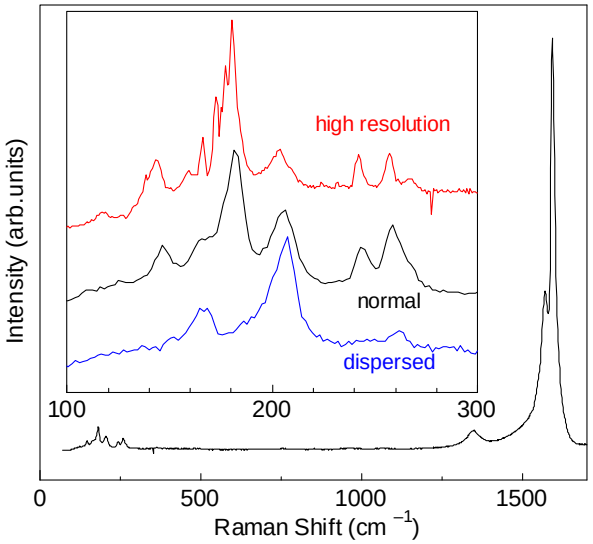

Fig. 2 Anomalous radial breathing mode of Raman scatterings excited from the top of a VA-SWNT film. Raman spectra taken from the top of a VA-SWNT array. Inset shows the RBM region with high-resolution (topmost) and with normal resolution before (middle) and after (lower) dispersion in D_2O.

bundling structure is ideal for various optical characterizations such as resonant Raman (22) and possible production of homogeneous composite materials (23). Optical characterization of such a film using polarized absorption, polarized Raman, and photoluminescence spectroscopy will be discussed. Laser-excitation of a vertically aligned film from top means that each nanotube is excited perpendicular to its axis. Because of this predominant perpendicular excitation,

interesting cross-polarized absorption (24) and interesting and practically important Raman features as shown in Fig. 2 are observed (25). Polarization-dependent resonance Raman spectra of VA-SWNT were measured such that the polarization of the scattered light was selected either parallel or perpendicular to that of the incident light. For the parallel configuration, radial breathing mode (RBM) peaks exhibited two different polarization dependencies. One group (dominated by a peak at 203 cm^{-1}) had a maximum scattering intensity for incident light parallel to the alignment direction, whereas the other group (dominated by a peak at 181 cm^{-1}) had maximum intensity for excitation perpendicular to the alignment direction. This anomaly has been attributed to resonance with non-vertical transitions due to perpendicularly polarized excitation before. Decomposing the Raman spectra and comparing to theoretical expectations for the two different configurations revealed that the 203 cm^{-1} group peaks behave as expected for parallel-polarized dipole excitation, whereas the 181 cm^{-1} group peaks deviate significantly from the prediction assuming perpendicularly polarized excitation. Furthermore, after correcting the spectra for laser-induced heating effects, the 181 cm^{-1} group peak intensities were found to be essentially independent of polarization angle. The sound interpretation of these results is that the RBM anomaly is due to the parallel excitation of 'stray' SWNTs suspended within the vertically aligned array.

GAS PHASE THERMAL DECOMPOSITION

The non-flow CVD (13) turned out to be very efficient, resulting a thicker film up to 100 µm. The growth curve is obviously different probably because of the contribution of small amount of acetylene thermally decomposed from ethanol (14). The carbon conversion rate from ethanol to VA-SWNTs can be as high as 40 %. Hence, isotopically modified ethanol can be employed to study the growth process (19). The detailed chemical reaction process in gas-phase and on metal catalysts will be discussed based on CVD results using isotope labeled ethanol and acetylene as carbon source.

We have previously investigated the influence of CVD temperature and pressure on the synthesis of VA-SWNTs by ACCVD (17). However, since ethanol thermally decomposes at typical growth temperatures (14), the actual catalyst environment can be significantly affected by the gas flow rate, even when the furnace temperature is unchanged. Fig. 3a shows the temperature profile based on a numerical calculation using the FLUENT software package for an ethanol flow rate of 450 sccm through a 60 cm furnace maintained at a temperature of 800 °C. The dashed oval indicates the position of the substrate, and is found to be approximately 20 °C cooler than the furnace temperature. Thermal decomposition of ethanol under these conditions was also calculated, and the concentrations of ethanol and various chemical species produced by its thermal decomposition are shown in Fig. 3c. Under these conditions, ethanol almost completely decomposes in 2.5 seconds. The residence time in the chamber, however, is

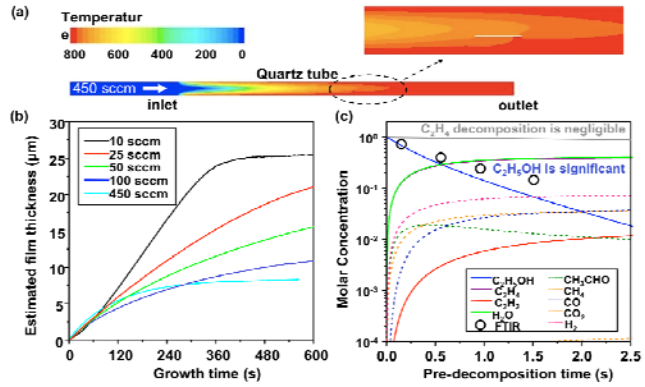

Fig. 3 (a) Temperature distribution inside the quartz tube during CVD. (b) Growth curves at 800 °C for different ethanol flow rates show a change for slow flow rates. (c) Ethanol decomposition curves calculated by CHEMKIN, and experimentally measured ethanol concentrations (circles) by FT-IR spectroscopy.

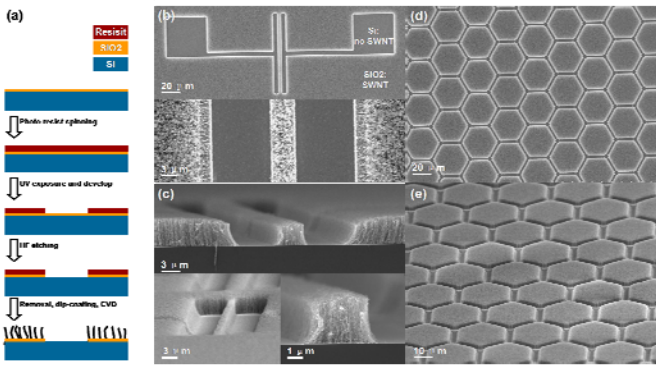

Fig. 4: (a) Schematic showing the substrate fabrication and selective growth; (b) Top and (c) side view SEM images of an electrode-shaped pattern, where SWNTs only grew in the SiO_2 regions. (d) Top and (e) side view images of hexagon-shaped patterns. The growth behavior of SWNTs at the edges is slightly different from in the center of a vertically aligned forest.

only 0.1 s, thus the ethanol concentration near the catalyst should be more than 90%. In the case of a slower flow rate the gas would be heated to the furnace temperature by the time it arrives at the substrate (due to the shorter entrance length), thus slightly increasing the local temperature at the catalyst. Much more importantly, a slower flow would increase the residence time of ethanol in the heated region. As a result, a more significant portion of the ethanol would have thermally decomposed before reaching the catalyst. This is evidenced experimentally by the growth curves presented in Fig. 3b, which correspond to different ethanol flow rates under otherwise identical conditions. As the flow rate decreases the catalyst lifetime increases significantly, enhancing SWNT growth. This is likely due to an increase in the production of

C_2H_4 and H_2O. In most cases the general growth behavior is typical exponential decay (17), but when the flow rate is very slow (i.e., <25 sccm) the growth process changes significantly, as shown by the topmost black curve in Fig. 3b. In this case the growth rate is nearly constant for approximately three minutes and then suddenly stops. This catalytic sudden-death has been reported elsewhere (26-28), but the mechanism still remains as an open question in this field.

PATTERNED GROWTH (SiO_2 –BASED PATTERN)

SWNT arrays were grown on SiO_2 patterned Si substrates using ethanol as a carbon source and Co as the catalyst. A 50 nm thick SiO_2 layer was patterned on a Si wafer using standard UV lithography combined with HF etching. A schematic showing the fabrication process is shown in Fig. 4a. The catalyst was loaded onto the substrate by the previously reported dip-coating process. The substrate was submerged into the dip-coating solution (0.1% wt. cobalt acetate in ethanol), soaked for 3 min, and withdrawn slowly at 4 cm/min. The substrate was then baked in air at 400 °C for 5 min before CVD. Only cobalt acetate was used here as the catalyst precursor because we recently found VA-SWNT arrays can still be obtained when Mo is absent, as long as the parameters are well optimized. ACCVD was performed at 700-800 °C with an ethanol flow of 450 sccm at a pressure of 1.3 kPa.

Figure 4b shows typical top-view SEM images of an electrode-shaped SWNT pattern (11). It is clear that SWNTs grow only in regions where an oxide layer is present. No growth was observed in areas where the oxide layer had been etched by HF. The SWNT structures can form lines, hexagons (Fig. 4d) or other shapes depending on the pre-designed pattern. The resolution of this method is limited by the ability of obtaining oxide area on a Si wafer. In this experiment, a linewidth of several micrometers was achieved using UV lithography. If other higher resolution techniques (e.g. electron-beam lithography, scanning probe oxidation) were used, finer SWNT structures may be obtained. The convenience in this approach is that the regions where SWNTs grow can be well controlled by pre-fabrication. Dip-coating was performed on the entire substrate and no further processing (e.g., lift-off) was needed.

The cross-sectional view of a pattern (Fig. 4c) confirmed the alignment of the obtained SWNTs. However, SWNTs can also grow into random networks if the catalyst density is significantly decreased. Both edges of a line pattern always exhibit transition regions, where the SWNTs are not perfectly perpendicular to the substrate. Apart from these few micrometers, however, the alignment is essentially the same as in VA-SWNT arrays. The formation of such transition regions is very likely due to the different wetting behavior of liquid at the edge. Further study is needed to understand and control this phenomenon.

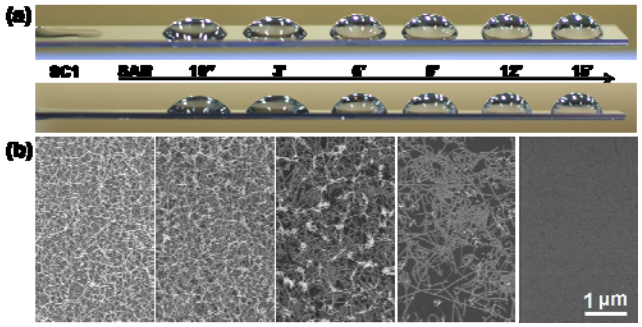

Fig. 5 (a) Various contact angles of water droplets on hydrophilic surface terminated by OH after standard cleaning 1 (SC1) and hydrophobic surface functionalized by OTS monolayer with different SAM converge; (b) SEM images of SWNTs grown on substrate shown in (a) after catalyst dip-coating.

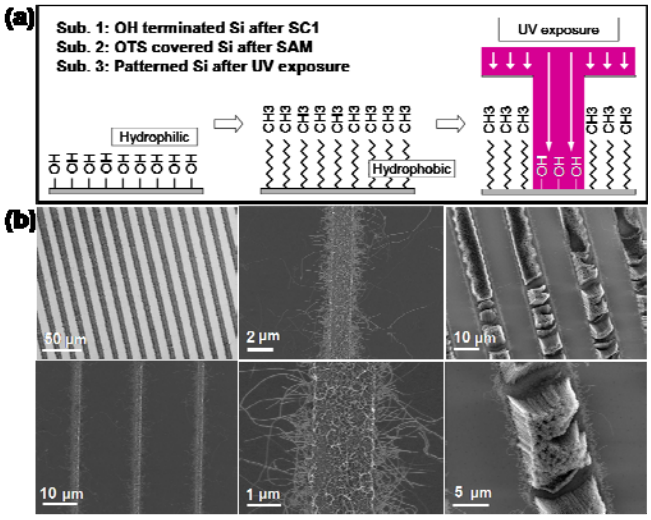

Fig. 6 (a) Schematics describing the fabrication procedure of hydrophilic/hydrophobic patterns using a selective removal of OTS SAM by UV exposure; (b) SEM images of random and vertically aligned SWNT line-shape patterns.

PATTERNED GROWTH (SAM-BASED PATTERN)

The effects of surface chemistry on the yield of SWNTs suggest the ability to control the growth position, which is critical to constructing 3-D vertically aligned SWNT structures or 2D SWNT patterns on a substrate (12). To selectively suppress growth created the opposite effect of plasma treatment, i.e. increased the hydrophobicity of the surface, by forming a SAM of octadecyltrichlorosilane (OTS) on the substrate surface (29). The terminating CH_3 group makes the surface superhydrophobic, increasing the contact angle of water from nearly 0 (for OH-terminated) to approximately 110°. After

dip-coating and CVD, almost no carbon structures were found on the substrate. The effects of these surface treatments are compared in Fig. 5, which shows that an OH-terminated surface significantly boosted the array height, while a CH_3-terminated surface effectively prevented SWNT synthesis.

The appeal of using an SAM lies in not only the easy fabrication and drastic change of surface energy (by only one layer of molecules), but also the reversibility of the SAM process. For example, deep UV light (here 254 nm) is known to be able to remove the SAM effectively. The exposed surface can retrieve its hydrophilicity (water contact angle returns to almost 0°) and SWNTs can efficiently grow on it. Therefore, by combining with a masking technique, silicon surfaces with sharp hydrophilic/hydrophobic patterns can be easily obtained. A schematic of this process is presented in Fig 6a. Line patterned SWNTs obtained after dip-coating and CVD are shown in Fig. 6b. Regions exposed to UV radiation after SAM formation clearly produced SWNTs with high density. On the other hand, no SWNTs grew in the masked areas, as no catalyst was deposited due to the high hydrophobicity of the surface. Importantly, the fabrication of patterned catalyst through this all-liquid route is both simpler and more efficient than conventional photolithography, as developing and removal of photoreisit is bypassed. Compared to the post-pattern techniques, which normally introduce some irreversible destruction and contamination (e.g. pre-dispersion with surfactant) to the SWNTs, these high-quality as-grown SWNTs are expected to give better performances in device applications.

DIFFUSIVE-BALLISTIC HEAT CONDUCTION

The diffusive-ballistic heat conduction of finite-length single-walled carbon nanotubes has been studied by means of nonequilibrium molecular dynamics simulations. The length dependence of thermal conductivity (30) is quantified for a range of nanotube lengths up to 1.6 μm at room temperature. A gradual transition from nearly pure ballistic to diffusive-ballistic heat conduction was identified from the thermal conductivity profile. In the diffusive-ballistic regime, the profile exhibits power-law length dependence and does not converge even for a tube length of 1.6 μm as shown in Fig. 7 (31). We also present a theoretical scheme that seamlessly handles the crossover from fully ballistic to diffusive thermal transport regimes (32). At room temperature, the micrometer-length nanotubes belong to the intermediate regime in which ballistic and diffusive phonons coexist, and the thermal conductance exhibits anomalous nonlinear tube-length dependence due to this coexistence. This result is in excellent agreement with molecular-dynamics simulation results showing the nonlinear thermal conductance.

The diffusive-ballistic phonon transport regime covers a wide range of nanotube-lengths in actual applications due to the extraordinary long phonon mean free path at room temperature. This gives rise to various unique stationary and non-stationary heat conduction characteristics (33, 34).

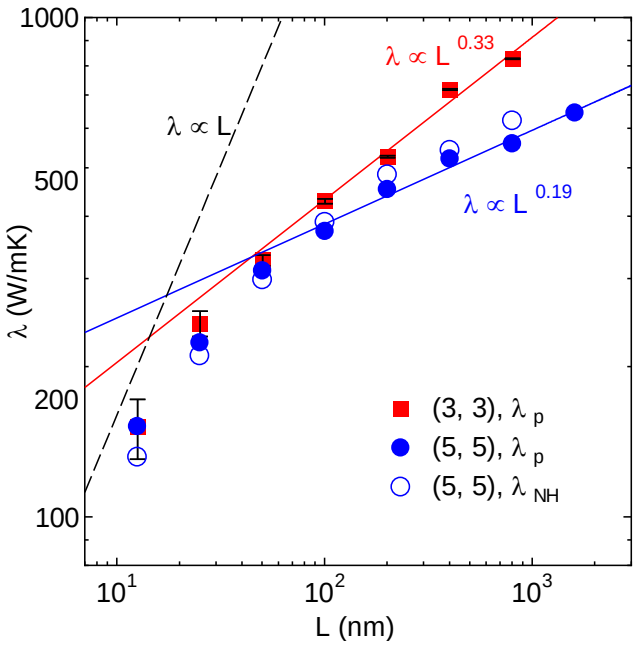

Fig. 7 Length dependences of SWNT thermal conductivity for two different diameters. λ_p and λ_{NH} denote the values obtained by using phantom and Nose-Hoover thermostats, respectively. The error bars are based on the fitting residuals in the thermal conductivity calculations. The residuals were largest in the case of (3, 3) SWNTs. The thermal conductivity profiles of (3, 3) and (5, 5) SWNTs for L>100 nm were fitted to power laws. The dashed line shows $\lambda \propto L$ with an arbitrary slope.

Furthermore, several issues of heat transfer in practical situations are studied by MD simulations (35).

ACKNOWLEDGMENTS

Part of this work was financially supported by Grant-in-Aid for Scientific Research (19206024 and 19054003) from the Japan Society for the Promotion of Science, SCOPE (051403009) from the Ministry of Internal Affairs and Communications, 'Development of Nanoelectronic Device Technology' of NEDO, and Global COE Program 'Global Center for Excellence for Mechanical Systems Innovation', MEXT, Japan.

REFERENCES

1. Y. Murakami, S. Chiashi, Y. Miyauchi, M. H. Hu, M. Ogura, T. Okubo, and S. Maruyama, *Chem. Phys. Lett.* **385**, 298 (2004).
2. S. Maruyama, R. Kojima, Y. Miyauchi, S. Chiashi, and M. Kohno, *Chem. Phys. Lett.* **360**, 229 (2002).
3. K. Hata, D. N. Futaba, K. Mizuno, T. Namai, M. Yumura, and S. Iijima, *Science* **306**, 1362 (2004).

4. G. Y. Zhang, D. Mann, L. Zhang, A. Javey, Y. M. Li, E. Yenilmez, Q. Wang, J. P. McVittie, Y. Nishi, J. Gibbons, and H. J. Dai, *Proc. Natl. Acad. Sci. U.S.A.* **102**, 16141 (2005).
5. G. F. Zhong, T. Iwasaki, K. Honda, Y. Furukawa, I. Ohdomari, and H. Kawarada, *Jpn. J. Appl. Phys.* **44**, 1558 (2005).
6. G. Eres, A. A. Kinkhabwala, H. Cui, D. B. Geohegan, A. A. Puretzky, and D. H. Lowndes, *J. Phys. Chem. B* **109**, 16684 (2005).
7. Y. Murakami, Y. Miyauchi, S. Chiashi, and S. Maruyama, *Chem. Phys. Lett.* **377**, 49 (2003).
8. S. Noda, H. Sugime, T. Osawa, Y. Tsuji, S. Chiashi, Y. Murakami, and S. Maruyama, *Carbon* **44**, 1414 (2006).
9. H. Sugime, S. Noda, S. Maruyama, and Y. Yamaguchi, *Carbon* **47**, 234 (2009).
10. M. H. Hu, Y. Murakami, M. Ogura, S. Maruyama, and T. Okubo, *J. Catal.* **225**, 230 (2004).
11. R. Xiang, E. Einarsson, H. Okabe, S. Chiashi, J. Shiomi, and S. Maruyama, *Jpn. J. Appl. Phys.*, **49**, 02BA03 (2010).
12. R. Xiang, T. Wu, E. Einarsson, Y. Suzuki, Y. Murakami, J. Shiomi, and S. Maruyama, *J. Am. Chem. Soc.*, **131**, 10344 (2009).
13. H. Oshima, Y. Suzuki, T. Shimazu, and S. Maruyama, *Jpn. J. Appl. Phys.* **47**, 1982 (2007).
14. R. Xiang, E. Einarsson, J. Okawa, Y. Miyauchi, and S. Maruyama, *J. Phys. Chem. C*, **113**, 7511 (2009).
15. S. Maruyama, E. Einarsson, Y. Murakami, and T. Edamura, *Chem. Phys. Lett.* **403**, 320 (2005).
16. E. Einarsson, M. Kadowaki, K. Ogura, J. Okawa, R. Xiang, Z. Zhang, Y. Yamamoto, Y. Ikuhara, and S. Maruyama, *J. Nanosci. Nanotechnol.* **8**, 6093 (2008).
17. E. Einarsson, Y. Murakami, M. Kadowaki, and S. Maruyama, *Carbon* **46**, 923 (2008).
18. R. Xiang, E. Einarsson, J. Okawa, T. Thurakitseree, Y. Murakami, J. Shiomi, Y. Ohno, and S. Maruyama, *J. Nanosci. Nanotech.*, **10**, 3901 (2010).
19. R. Xiang, Z. Zhang, K. Ogura, J. Okawa, E. Einarsson, Y. Miyauchi, J. Shiomi, and S. Maruyama, *Jpn. J. Appl. Phys.* **47**, 1971 (2008).
20. E. Einarsson, H. Shiozawa, C. Kramberger, M. H. Rummeli, A. Gruneis, T. Pichler, and S. Maruyama, *J. Phys. Chem. C* **111**, 17861 (2007).
21. Y. Murakami and S. Maruyama, *Chem. Phys. Lett.*, **422**, 575 (2006).
22. P. T. Araujo, S. K. Doorn, S. Kilina, S. Tretiak, E. Einarsson, S. Maruyama, H. Chacham, M. A. Pimenta, and A. Jorio, *Phys. Rev. Lett.*, **98**, 067401 (2007).
23. H. M. Duong, D. V. Papavassiliou, K. J. Mullen and S. Maruyama, *J. Phys. Chem. C*, **112**, 19860 (2008).
24. Y. Miyauchi, M. Oba and S. Maruyama, *Phys. Rev. B*, **74**, 205440 (2006).
25. Z. Zhang, E. Einarsson, Y. Murakami, Y. Miyauchi and S. Maruyama, *Phys. Rev. B*, **81**, 165442 (2010).
26. R. Andrews, D. Jacques, D. Qian, and T. Rantell, *Acc. Chem. Res.* **35**, 1008 (2002).
27. E. R. Meshot, and A. J. Hart, *Appl. Phys. Lett.* **92**, 113107 (2008).
28. D. B. Geohegan, A. A. Puretzky, I. N. Ivanov, S. Jesse, G. Eres, and J. Y. Howe, *Appl. Phys. Lett.* **83**, 1851 (2003).
29. A. Ulman, *Chem. Rev.* **96**, 1533 (1996).
30. S. Maruyama, *Physica B*, **323**, 193 (2002).
31. J. Shiomi, and S. Maruyama, *Jpn. J. Appl. Phys.*, **47**, 2005(2008).
32 T. Yamamoto, S. Konabe, J. Shiomi and S. Maruyama, *Appl. Phys. Express*, **2**, 095003 (2009).
33. J. Shiomi, and S. Maruyama, *Phys. Rev. B*, **74**, 155401 (2006).
34. J. Shiomi, and S. Maruyama, *Phys. Rev. B*, **73**, 205420 (2006).
35. S. Maruyama, Y. Igarashi, Y. Taniguchi, and J. Shiomi, *J. Therm. Sci. Tech.*, **1**, 138 (2006).